AGU PUBLICATIONS

Geophysical Research Letters

RESEARCH LETTER

10.1002/2017GL074188

Key Points:
- Multidecadal variations in European winter precipitation are linked to North Atlantic atmospheric circulation changes
- A new pattern of winter precipitation emerged over the British Isles in recent decades
- Recent precipitation changes over the British Isles coincide with shifts in storm tracks and atmospheric rivers

Supporting Information:
- Supporting Information S1

Correspondence to:
C. C. Ummenhofer,
cummenhofer@whoi.edu

Citation:
Ummenhofer, C. C., H. Seo, Y.-O. Kwon, R. Parfitt, S. Brands, and T. M. Joyce (2017), Emerging European winter precipitation pattern linked to atmospheric circulation changes over the North Atlantic region in recent decades, *Geophys. Res. Lett.*, *44*, doi:10.1002/2017GL074188.

Received 18 MAY 2017
Accepted 20 JUL 2017
Accepted article online 25 JUL 2017

Emerging European winter precipitation pattern linked to atmospheric circulation changes over the North Atlantic region in recent decades

Caroline C. Ummenhofer[1], Hyodae Seo[1], Young-Oh Kwon[1], Rhys Parfitt[1], Swen Brands[2], and Terrence M. Joyce[1]

[1]Department of Physical Oceanography, Woods Hole Oceanographic Institution, Woods Hole, Massachusetts, USA, [2]MeteoGalicia—Xunta de Galicia, Consellería de Medio Ambiente e Ordenación do Territorio, Santiago de Compostela, Spain

Abstract Dominant European winter precipitation patterns over the past century, along with their associated extratropical North Atlantic circulation changes, are evaluated using cluster analysis. Contrary to the four regimes traditionally identified based on daily wintertime atmospheric circulation patterns, five distinct seasonal precipitation regimes are detected here. Recurrent precipitation patterns in each regime are linked to changes in atmospheric blocking, storm track, and sea surface temperatures across the North Atlantic region. Multidecadal variability in the frequency of the precipitation patterns reveals more (fewer) winters with wet conditions in northern (southern) Europe in recent decades and an emerging distinct pattern of enhanced wintertime precipitation over the northern British Isles. This pattern has become unusually common since the 1980s and is associated with changes in moisture transport and more frequent atmospheric river events. The observed precipitation changes post-1950 coincide with changes in storm track activity over the central/eastern North Atlantic toward the northern British Isles.

1. Introduction

Recent unusual wintertime climatic conditions in Europe and other midlatitude regions have received increasing attention [e.g., *Francis and Vavrus*, 2012; *Cohen et al.*, 2014; *Screen and Simmonds*, 2014]. Wintertime variability in the North Atlantic region is dominated by distinct weather regimes, such as the two phases of the North Atlantic Oscillation (NAO), the Atlantic Ridge, and European Blocking, which exert pronounced impacts on regional climate [*Vautard*, 1990; *Hurrell*, 1995; *Cassou et al.*, 2004; *Hurrell and Deser*, 2009]. Such recurrent regimes are often determined based on cluster analysis of wintertime sea level pressure (SLP), which can reveal nonlinear or asymmetric features in dominant wintertime circulation regimes. Alternatively, leading modes of SLP can be identified using Empirical Orthogonal Function (EOF) analysis, though caution is warranted when interpreting EOF patterns [e.g., *Dommenget and Latif*, 2002], given that they do not necessarily represent physical/dynamical modes of the climate system. Both approaches robustly reveal the NAO as the leading mode of variability across the North Atlantic region. In contrast, the spatial expression and temporal characteristics of additional wintertime circulation patterns are sensitive to the analysis domain and period due to low-frequency modulations in the North Atlantic ocean-atmosphere system. *Hurrell and Deser* [2009] further highlight the considerable within-season variance in the atmospheric circulation of the North Atlantic as a limitation of regime-based approaches making it difficult to characterize winters as falling into one single circulation pattern or NAO phase.

Here to understand variability and change in European wintertime precipitation and the accompanying circulation and oceanic changes across the broader North Atlantic region, we focus on characteristic European precipitation patterns and assess multidecadal variations in their frequency over time. By combining a rigorous statistical analysis and dynamical interpretations, the study aims at providing new insights into links between North Atlantic extratropical variability and observed low-frequency changes in winter precipitation over Europe. It is noted that by design this study focuses on recurring wintertime *precipitation*—not *circulation*—patterns and changes in their frequency over time. Thus, while links to dominant climate modes (e.g., NAO) are likely, one would not necessarily expect precipitation patterns to be explained solely by one specific circulation mode or weather regime [e.g., *Hurrell and Deser*, 2009; *Gastineau et al.*, 2013, and references therein].

According to *Scaife et al.* [2008] heavy winter precipitation events in northern Europe are 50% more likely during sustained positive NAO periods than during its negative phase, with implications for UK flooding events [*Huntingford et al.*, 2014]. *Maidens et al.* [2013] found the winter of 2010/2011 with record-breaking low temperatures across northern Europe to coincide with an anomalously negative NAO phase and intense atmospheric blocking. They attributed the success in predicting the exceptional 2010/2011 wintertime conditions by October 2010 to anomalous ocean heat content and associated North Atlantic sea surface temperature (SST). Similarly, *Keenlyside and Omrani* [2014] suggested that warm North Atlantic SST associated with the Atlantic Multidecadal Oscillation (AMO) contributed to recent cold European winters, as positive AMO phases are associated with more negative NAO episodes [*Peings and Magnusdottir*, 2014; *Gastineau and Frankignoul*, 2015]. *Huntingford et al.* [2014] also implicated wetter conditions in northern Europe with changes in the AMO, as its warm phase is associated with higher precipitation across the Eastern Atlantic [*Alexander et al.*, 2014]. This suggests that extratropical ocean conditions may influence atmospheric conditions, especially on multidecadal time scales, while the converse occurs at shorter time scales [*Gulev et al.*, 2013].

Leading modes of variability, such as the NAO and AMO, often exert their impact on European winter climate through modulation of atmospheric blocking activity over the North Atlantic-European sector [e.g., *Scherrer et al.*, 2006; *Croci-Maspoli et al.*, 2007; *Häkkinen et al.*, 2011; *Davini et al.*, 2015; *Luo et al.*, 2015]. Atmospheric blocking represents a prominent weather phenomenon in the extratropics: During a blocking situation, the large-scale midlatitude zonal flow is impeded and meridional anomalies occur in the upper level jet; the anomalous circulation pattern remains largely stationary, generally persists for several days at a time, and is often associated with extreme events [e.g., *Coumou and Rahmstorf*, 2012]. For example, a strong anticyclone over Scandinavia and eastward extension of the North Atlantic storm track were implicated in the severe flooding in England and Wales in autumn 2000 [*Pall et al.*, 2011]. European extreme wintertime hydroclimatic events have also been linked to atmospheric rivers (AR) [e.g., *Zhu and Newell*, 1994; *Gimeno et al.*, 2014]. These phenomena are channels of intense horizontal water vapor transport in the lower troposphere that are mainly fed by local moisture convergence along the cold front of an extratropical cyclone [*Dacre et al.*, 2015]. If seen in satellite imagery or reanalysis data, these elongated structures are often reminiscent of the meanders formed by a river and can be thousands of kilometers long [e.g., *Brands et al.*, 2017]. While AR-associated precipitation totals—often enhanced through orographic uplift [*Gimeno et al.*, 2014]—are lower further inland, they account for the majority of flooding events in the UK [e.g., *Lavers et al.*, 2011, 2012] and more broadly for heavy precipitation at the upper tail of the distribution over western Europe [*Lavers and Villarini*, 2013]. The unusually stormy and wet winter of 2013/2014 over the UK coincided with an intensified and eastward extended North Atlantic storm track, whose persistence in that position was linked to warm tropical Atlantic conditions [*Huntingford et al.*, 2014; *Kendon and McCarthy*, 2015].

2. Data and Methods

Monthly gridded observational/reanalysis products were used to assess regional hydroclimate and circulation conditions. At 2° horizontal resolution, these included SLP, air temperature, winds, and geopotential height from the twentieth century reanalysis v2c (20CR; 1871–2012) [*Compo et al.*, 2011]; SST at 1° resolution from the UK Hadley Centre HadISST v1.1 (1870–present) [*Rayner et al.*, 2003]; and precipitation at 0.5° resolution from the Global Precipitation Climatology Centre v6 (GPCC; 1901–2010) [*Schneider et al.*, 2014]. The common analysis period was 1901–2010. However, results are consistent for the more recent period post-1979 with improved data coverage using the European Centre for Medium range Weather Forecasting reanalysis product (ERA-Interim; 1979–present) [*Uppala et al.*, 2005], precipitation from the Climate Prediction Center (CPC) Merged Analysis product (CMAP; 1979–present) [*Xie and Arkin*, 1996] and the ENSEMBLES daily gridded observational product (E-OBS v15.0; 1950–present) [*Haylock et al.*, 2008], and NOAA Optimum Interpolation SST v2 (1982–present) [*Reynolds et al.*, 2002], as seen in supporting information Figure S6. Given the robustness of the results, we also only show the longer period 1901–2010 based on the 20CR ensemble mean, as the ensemble spread in the reanalysis among its 56 ensemble members is small for key metrics, such as wintertime blocking days or position of the eddy-driven jet.

The limited availability and spatial coverage of long-term high-quality daily European precipitation station data prior to the 1950s makes it difficult to assess long-term trends in precipitation extremes [e.g., *KleinTank and Können*, 2003; *Zolina et al.*, 2005, 2014], compared to mean precipitation changes [*Zolina et al.*, 2009]. Our study therefore focuses on seasonal precipitation totals using the GPCC gridded product, rather than daily extremes, and on year-to-year variations for seasonal precipitation averages, rather than long-term trends. For details see supporting information S1 [*Uppala et al.*, 2005; *Haylock et al.*, 2008; *Huffman et al.*, 2009; *Dee et al.*, 2011]. Analyses are based on the January–March (JFM) season, as European wintertime precipitation exhibits similar spatiotemporal features in the long-term mean and variability, whether focusing on JFM or December–February (not shown).

Hierarchical cluster analysis was used to identify recurrent states (or regimes) of European precipitation by grouping them according to an objective similarity criterion, without an a priori determination of the number of clusters. We performed Ward's cluster method [*Ward*, 1963] as described by *Cheng and Wallace* [1993] on detrended area-weighted anomaly maps of JFM precipitation. Five dominant patterns of precipitation were identified by the clustering algorithm. The years for each cluster are listed in Table S1 and their temporal evolution in Figures 3 and S8.

Blocking days over the region 30°–70°N were calculated for 20CR following the method by *Scherrer et al.* [2006] and *Häkkinen et al.* [2011] and refer to the number of days per season that exhibit blocking conditions at each gridpoint based on the meridional gradient of the daily geopotential height at 500 hPa. Variations in the number of blocking days could result from a change in the duration of blocking events or their number. For details, see supporting information S2 [*Rex*, 1950; *Woollings et al.*, 2008; *Davini et al.*, 2012]. Storm track activity is measured by the covariance of band-pass filtered daily v and T at 850h Pa, (i.e., $< v'T' >$) using a sixth-order Butterworth filter.

Wintertime AR events are detected with the algorithm described in *Brands et al.* [2017]. This algorithm operates on the intensity (IVT) and direction (D) of the vertically integrated water vapor transport (IVT) obtained from 20CR and is applied for the eight target regions displayed in supporting information Figure S2. For a given target region and instant of time, the algorithm first queries whether the IVT is anomalously strong and then "crawls" up the flow until IVT falls below a certain threshold. If the detected structure is longer than 3000 km, the region is affected by an AR at that instant in time. Thereby, six-hourly AR occurrence-absence time series are obtained which are then accumulated for each JFM season to yield year-to-year AR count series describing the AR-activity in that region. A more detailed description of the algorithm is provided in supporting information S2.

3. Wintertime European Precipitation Patterns and Links to Regional Circulation

A cluster analysis performed on JFM precipitation reveals recurrent anomaly patterns across Europe (Figure 1a). Pattern A is characterized by anomalously dry conditions for the British Isles, southern Norway and Sweden, and northern central Europe. In pattern B, anomalous wet conditions in excess of +20 mm/month are observed over the British Isles, western, central, and parts of eastern Europe, as well as southern Norway and Sweden. Pattern C is characterized by very wet conditions for southern and western Europe, including the British Isles with the exception of Scotland, which exhibits anomalous dry conditions, as does Norway. Pattern D is the opposite to pattern C with a severe reduction in precipitation (<−40 mm/month) for southern and western Europe, while Norway records wet anomalies in excess of +50 mm/month. Pattern E is strikingly similar overall to cluster D, except for the British Isles: in pattern D, the British Isles, with the exception of Scotland, are characterized by significant reductions in precipitation. In pattern E, on the other hand, Ireland and Scotland experience anomalously wet conditions in excess of +50 mm/month, while southeastern England is anomalously dry.

Pattern A is characterized by a weakened meridional pressure gradient with anomalous high SLP extending from Iceland toward Scandinavia and reduced SLP south of 50°N (Figure 1b). Pattern B broadly exhibits anomalies of the opposite sign to A. Comparing the SLP anomalies in Figure 1b with the traditional daily weather regimes or EOF-based circulation patterns [*Vautard*, 1990; *Cassou et al.*, 2004; *Hurrell and Deser*, 2009] reveals that while certain features of the positive/negative NAO or ridge pattern are present—a one-to-one correspondence is challenging. This is not surprising given that one would not expect JFM precipitation to be purely dominated by one circulation type given the considerable within-season variance and limitations with the EOF- or regime-based approaches identified earlier [e.g., *Hurrell and Deser*, 2009].

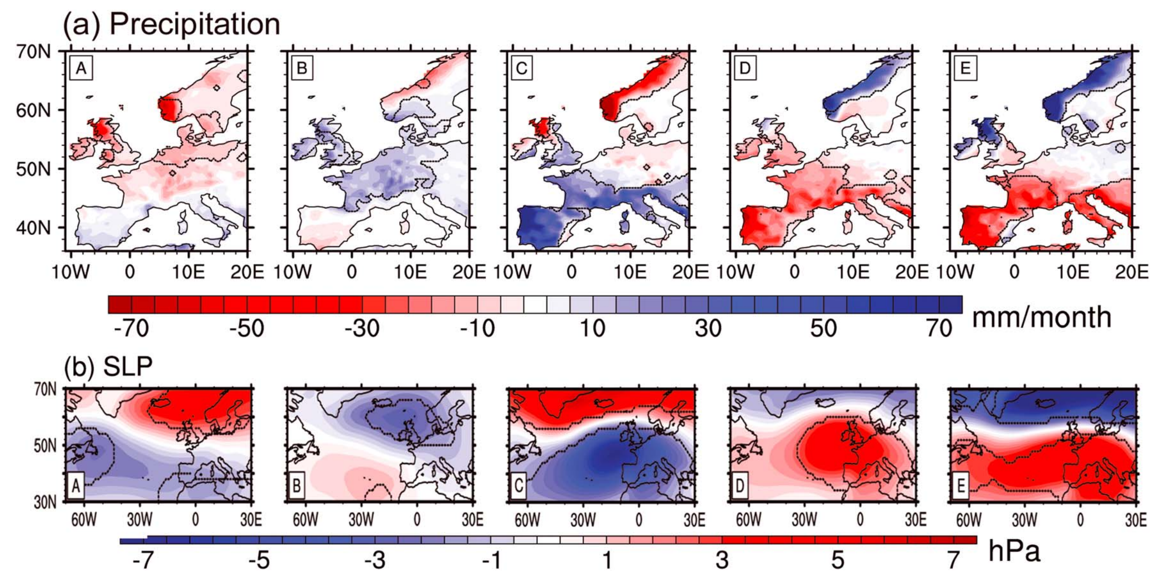

Figure 1. (a) Composite anomalies of precipitation (mm/month) clustered for the European region, along with (b) the associated SLP (hPa) anomalies, both for JFM for the period 1901–2010. The area enclosed by the black contours denotes anomalies that are significant at the 2% significance level as estimated by Student's *t* test.

The results indicate that subtle differences in the SLP patterns can yield relatively large differences in the precipitation distribution (e.g., British Isles). To understand these differences in the circulation anomalies characterizing precipitation clusters D and E, we composite the detrended JFM anomalies for the same years for related fields, such as surface winds, atmospheric blocking, storm track activity, and SST (Figure 2).

4. Emergence of Distinct Wintertime Precipitation Pattern Over the British Isles in Recent Decades

Pattern D is characterized by a strengthening and northward shift in the westerly flow and storm track activity over Europe north of 50°N (Figures 2a–2c). This coincides with enhanced blocking activity over the eastern Atlantic and centered over the British Isles and western central Europe. In pattern E, an albeit not significant reduction in blocking extends from Greenland across the northern tier into Europe. Over the British Isles, pattern E is associated with a significant southward displacement of the enhanced storm track activity compared to D, where the significant strengthening of $< v'T' >$ is located north of the British Isles (Figures 2b and 2c). The latter accounts for the distinct wintertime precipitation signal over the northern British Isles, with dry conditions across the entire British Isles when the storm track is shifted to the north of the country (D), while northern Ireland, northern England, and Scotland experience wet conditions during enhanced storm track activity further south (E). A significant enhancement in the North Atlantic storm track, including over the British Isles, (Figure 2c) thus results in significant regional precipitation changes over the northern British Isles. Interestingly, the anomaly patterns of SST across the North Atlantic region are very distinct: pattern D exhibits anomalously warm SST for much of the North Atlantic. In contrast, pattern E is characterized by warm SST anomalies over the eastern Atlantic and European shelf areas, while anomalous cold SST dominate the subpolar northwest Atlantic. Turbulent heat flux anomalies (Figure S4) indicate negative correlations with the SST anomalies; i.e., reduced heat flux out of the ocean corresponds to warmer SST, indicative of the atmosphere forcing the ocean, consistent with the findings of *Gulev et al.* [2013] for interannual time scales.

AR events play an important role in heavy precipitation events in the midlatitudes along the Atlantic eastern seaboard [*Gimeno et al.*, 2014]. Given the distinct precipitation patterns in clusters D and E over the British Isles, Figure 2e further explores the role of IVT and the frequency of occurrence of AR events along the eastern Atlantic seaboard for the two clusters. Both clusters are characterized by significant reductions in IVT across the subtropical North Atlantic and extending onto Europe, mirrored by reduced occurrence of AR events for the Iberian Peninsula and France (Figure 2e). Consistent with the precipitation in pattern D, extensive and significant increases in IVT anomalies occur only at the very northern edge of the British Isles toward Iceland. In contrast, pattern E exhibits very strong enhanced IVT anomalies over the British Isles, also reflected

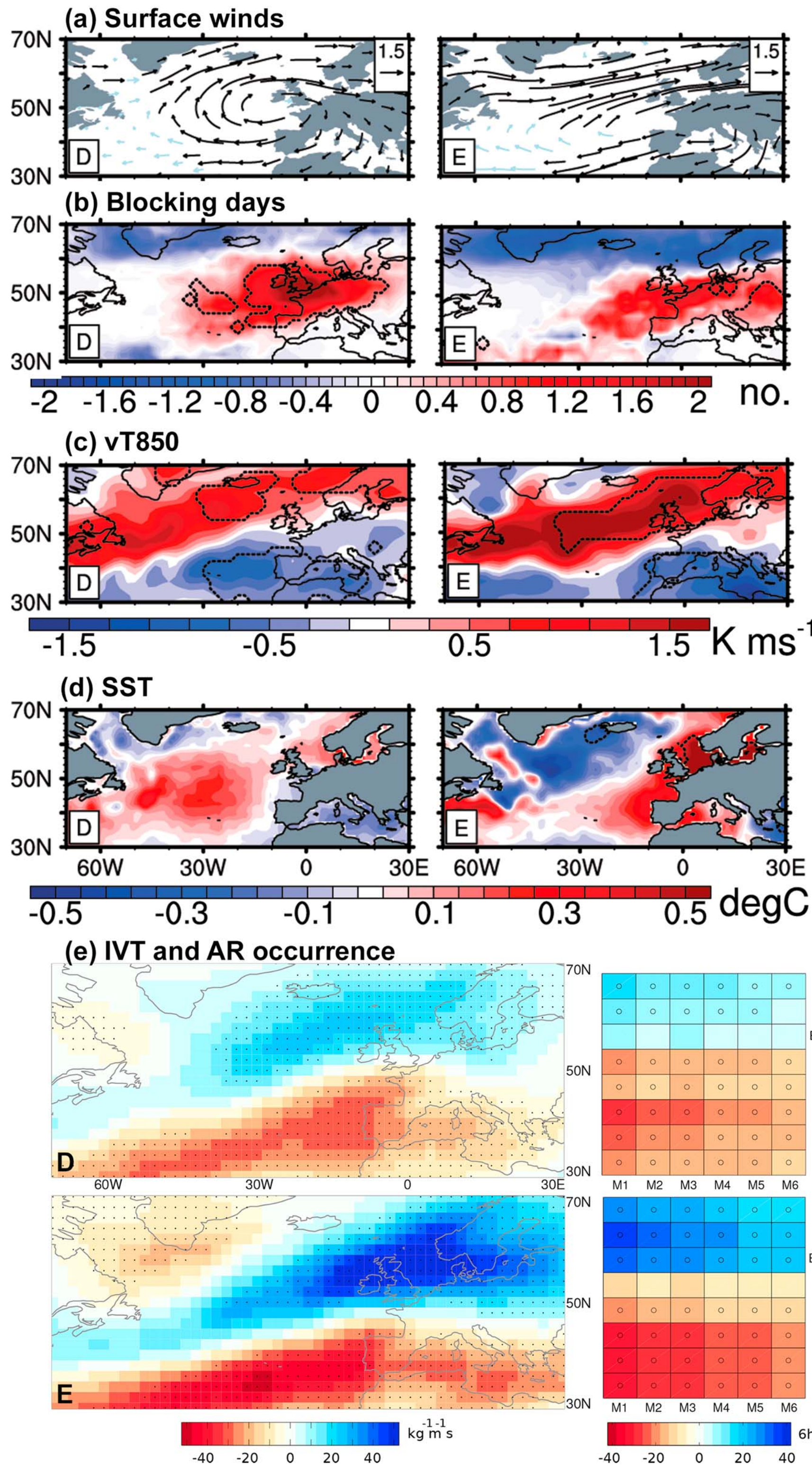

Figure 2. Composite anomalies of (a) surface winds (m/s), (b) number of blocking days per season, (c) 2–6 day band-pass filtered $< v'T' >$ at 850 hPa (K m/s), (d) SST (°C), and (e, f) integrated water vapor transport (IVT; kg/m/s) and atmospheric river (AR) occurrence, all for JFM for the period 1901–2010 for years in clusters D and E. Count of occurrence of AR events for eight target regions along the eastern Atlantic seaboard. Dashed contours and black vectors in Figures 2a–2d and stippling/circles in Figures 2e and 2f denote anomalies significant at the 2% significance level as estimated by Student's *t* test. M1 to M6 represent the six method modifications of *Brands et al.* [2017] using different percentile thresholds to define an AR.

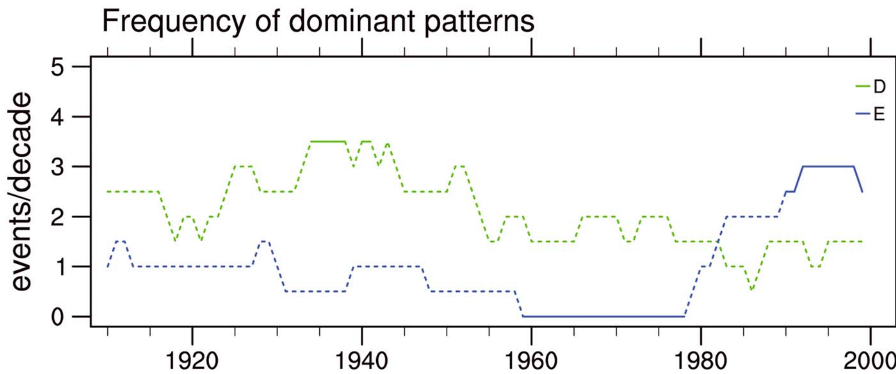

Figure 3. Running average of the number of events in the JFM precipitation clusters D and E per decade for the period 1901 – 2010. (NB: the value for each decade is plotted with the year at the center of the decade.) Solid lines indicate periods when the number of events/decade is significantly different from average occurrence rates at the 5% significance level (as estimated by Monte Carlo testing).

in significantly more frequent AR events for the British Isles (Figure 2e). AR events occur significantly more frequently over Norway in both patterns D and E. These results are in agreement with the changes in atmospheric circulation and the storm track (Figures 2a – 2c).

The frequency of the dominant JFM precipitation patterns described here varied over time. The number of events, i.e., how often a winter was classified as exhibiting a particular pattern D or E in each decade, is shown in Figure 3 for the period 1901 – 2010. Multidecadal variations in the frequency of occurrence of these two different regimes are apparent: Pattern D occurred unusually often (in excess of three times per decade) in the 1930s and 1940s. In contrast, it was observed only rarely (less than once per decade) in the 1980s (Figure 3). Pattern E occurred very rarely during the period 1960 – 1980, while it has become much more common with 2 – 3 winters per decade since 1990 (Figure 3).

5. Circulation Changes Across the North Atlantic Region

Given the striking changes in the frequency of JFM precipitation patterns D – E over the second half of the twentieth century, with large implications for wintertime hydroclimatic conditions across Europe, difference fields for the period 1981 – 2010 relative to 1951 – 1980 are shown in Figure 4. The period 1981 – 2010 was characterized by significant reductions in JFM precipitation across the Iberian Peninsula, southern France, and northern Italy, while northern Germany, the Benelux States, Denmark, western Norway, Sweden, as well as the northern British Isles experienced significantly wetter conditions (Figure 4). Over the British Isles, the increasing frequency of pattern E in the more recent 30 year period (Figure 3) can account for the increasingly wetter conditions over the British Isles.

The large-scale SLP change and associated surface winds across the broader North Atlantic region are consistent with a low-frequency shift in the NAO toward a more positive phase post-1980 (Figure 4b) and the associated regional precipitation changes [*Hurrell*, 1995]. Significant changes in blocking activity over the North Atlantic sector occurred as well, with Greenland blocking reduced by 1 – 1.5 days/season averaged over the JFM season, while blocking over the Azores increased by 1.5 days/season (Figure 4c). On the other hand, the blocking activity over the British Isles, albeit reduced, did not change significantly, consistent with *Barnes et al.* [2014]. *Barnes and Polvani* [2013] related these changes to the eddy-mean flow feedback, which implies that the position of the jet and frequency of poleward and equatorward wave breaking are strongly coupled. The storm track activity indicates an eastward extension relative to its mean track position toward the northern British Isles (Figure 4d), consistent with increased winter precipitation and enhanced AR incidence there in recent decades [*Huntingford et al.*, 2014, and references therein]. The eastward extension in the storm track might be associated with a shift in the NAO toward its positive phase during the period 1980 – 2000 and strengthened eastward (weakened westward) component of the North Atlantic storm track [*Luo et al.*, 2015]. These changes are in line with a northward shift in the jet stream, in agreement with the stronger zonal flow over the North Atlantic in a warmer climate with an intensified and less wobbly jet stream predicted by many climate models [e.g., *Barnes and Polvani*, 2013]. The North Atlantic SST in the more recent 30 year period were

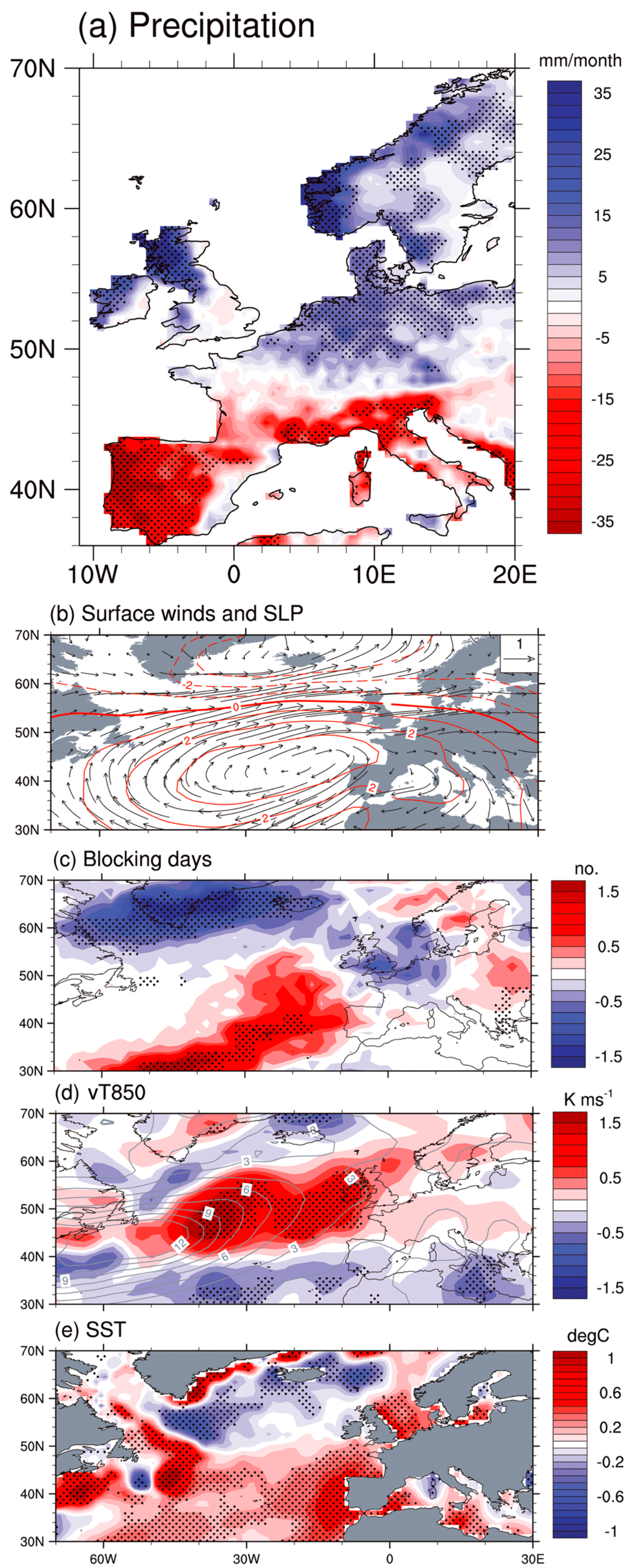

Figure 4. Difference in JFM fields for the period 1981–2010, relative to 1951–1980, for (a) precipitation (mm/month), (b) SLP (hPa; colored) and surface winds (m/s; vectors), (c) number of blocking days per season, (d) 2–6 day band-pass filtered $< v'T' >$ at 850 hPa (K m/s; colored difference; contours long-term mean), and (e) SST (°C). Stippling denotes differences significant at the 2% significance level according to Monte Carlo testing.

characterized by warm anomalies south of 50°N, the European Seas, Labrador Sea, and along the eastern Greenland coast, while the subpolar North Atlantic 50° – 70°N, 0 – 45°W was anomalously cold (Figure 4e). As such, the change in SST over the past 60 years reflects changes in the incidence of pattern E.

6. Summary and Conclusions

Dominant European winter precipitation patterns over the past century, along with their associated extratropical North Atlantic circulation changes, were evaluated using cluster analysis. Contrary to the four regimes traditionally identified based on wintertime daily atmospheric circulation patterns [e.g., *Cassou et al.*, 2004], five distinct precipitation regimes were detected here, because we focused on recurring wintertime seasonal mean *precipitation*—not daily *circulation*—patterns and changes in their frequency over time. Thus, some resemblance to circulation-based regimes or climate modes is likely. However, one would not necessarily expect seasonal mean precipitation patterns to be explained solely by the four dominant daily circulation regimes described by *Vautard* [1990] or *Cassou et al.* [2004].

Using various reanalysis products for the period 1901 – 2010, we assessed interannual to multidecadal variations in the frequency of these characteristic European wintertime precipitation patterns and links to accompanying changes in atmospheric blocking, moisture transport, storm track activity, and oceanic conditions. Five recurrent precipitation patterns were found, including an emergent precipitation pattern over the British Isles in recent decades. The related precipitation pattern D exhibited dry conditions for much of southern and central Europe and the British Isles. It was characterized by a strengthened meridional pressure gradient and northward displacement of the storm track, including northward displacement of ARs toward the Norwegian coast. In contrast, pattern E was associated with wet conditions over the northern British Isles driven by enhanced moisture transport and more frequent AR incidence along the west coasts of the British Isles and Norway.

Leading modes of North Atlantic climate variability, such as the NAO, Eastern Atlantic Pattern (EAP), and AMO, exert considerable impact on European winter hydroclimate across a range of time scales [e.g., *Hurrell*, 1995; *Hurrell and Deser*, 2009; *Alexander et al.*, 2014], often mediated through atmospheric circulation anomalies associated with blocking activity, storm track variability, and AR events over the North Atlantic-European sector.

As such, multidecadal variations in the frequency of occurrence of the respective precipitation regimes exhibit some consistency with low-frequency variations in leading modes of circulation variability in the North Atlantic region: Pattern D occurred unusually often (in excess of three times per decade) in the 1930s and 1940s, coinciding with a positive phase in the AMO. In contrast, it was observed only rarely (less than once per decade) in the 1980s during the negative phase of the AMO. The SST anomaly pattern associated with this cluster D is consistent with a positive phase of the AMO, indicating a warmer North Atlantic (Figure 2d). The 1960s – 1980s were characterized by unusually few winters with pattern E. This coincides with anomalous low or neutral phases in the NAO index around 1960s – 1970s, consistent with the spatial patterns in Figure 2. Pattern E has become more common with two to three events per decade since 1990, coinciding with a shift toward a more positive NAO post-1980 [*Hurrell*, 1995]. Changes in the frequency of patterns D and E thus likely reflect a combination of large-scale wintertime changes in the eddy-driven jet stream associated with the NAO and EAP [*Woollings et al.*, 2010; *Woollings and Blackburn*, 2012]. The results also show that subtle differences in the atmospheric circulation patterns yield relatively large differences in the precipitation distribution over the UK [*Kendon and McCarthy*, 2015] and in subpolar North Atlantic SST.

Considering Europe as a whole, the changes in the frequency of large-scale circulation patterns and resulting precipitation regimes are reflected in fewer winters with wet conditions in southern Europe but more in northern Europe; this is associated with a stronger storm track over the central and eastern North Atlantic toward the northern British Isles, weaker storm track activity south of 40°N, and corresponding changes in blocking activity over recent decades.

Similarly, *Fleig et al.* [2014] found changes in the frequency of dominant circulation patterns, rather than hydrothermal changes within circulation types, to contribute to wetting (drying) trends in northern (southern) Europe. These contributions were most pronounced for the JFM season and northwestern Europe. Multidecadal variations in dominant precipitation regimes, and their low-frequency modulation by North Atlantic modes of variability, such as NAO, EAP, and AMO, through effects on the large-scale circulation, likely contributed to observed changes in wintertime hydroclimate across Europe: Wintertime precipitation across Europe has sustained considerable trends over the past century [e.g., *Moberg et al.*, 2006; *Christensen et al.*, 2013; *Zolina et al.*, 2013; *Macdonald*, 2014; *Spinoni et al.*, 2015], with central, western, and northern Europe having become significantly wetter, while southern Europe sustained significant drying [*IPCC*, 2013]. However, as subtle differences in precipitation patterns D and E shown here demonstrate, it is not sufficient to look at changes in leading circulation patterns and/or associated climate modes to spot this emergent pattern of precipitation and SST that potentially greatly affects UK wintertime precipitation [*Huntingford et al.*, 2014], especially also in light of projected increases in AR frequency by the end of the 21st century for the latitude range 45°–55°N over western Europe [*Gao et al.*, 2016].

Acknowledgments
Use of the following data sets is gratefully acknowledged: Global Precipitation Climatology Center data by the German Weather Service (DWD) accessed through http://gpcc.dwd.de; Hadley Centre HadISST by the UK Met Office; CMAP and NOAA OI SST v2 data provided by NOAA/OAR/ESRL PSD, Boulder, Colorado, USA, through their website http://www.cdc.noaa.gov; the 20CR Project supported by the U.S. DOE, Office of Science Innovative and Novel Computational Impact on Theory and Experiment program, and Office of Biological and Environmental Research, and by the NOAA Climate Program Office; and the E-OBS data set from the EU-FP6 project ENSEMBLES (http://ensembles-eu.metoffice.com) and the data providers in the ECA&D project (http://www.ecad.eu). Comments by three anonymous reviewers helped to improve an earlier version of the manuscript. This research was supported by the U.S. National Science Foundation under AGS-1355339. Y.O.-K., H.S., and T.M.J. were also supported by the NASA Physical Oceanography Program under NNX13AM59G, R.P. by a *Weston Howland Jr.* Postdoctoral Scholarship, and C.C.U. by the *Investment in Science Fund given primarily by WHOI Trustee and Corporation Members* at WHOI.

References

Alexander, M. A., K. H. Kilbourne, and J. A. Nye (2014), Climate variability during warm and cold phases of the Atlantic Multidecadal Oscillation (AMO) 1871–2008, *J. Mar. Syst.*, *133*, 14–26.

Barnes, E. A., and L. Polvani (2013), Response of the midlatitude jets, and of their variability, to increased greenhouse gases in the CMIP5 models, *J. Clim.*, *26*, 7117–7135.

Barnes, E. A., E. Dunn-Sigouin, G. Masato, and T. Woollings (2014), Exploring recent trends in Northern Hemisphere blocking, *Geophys. Res. Lett.*, *41*, 638–644, doi:10.1002/2013GL058745.

Brands, S., J. M. Gutierrez, and D. San Martin (2017), Twentieth-century atmospheric river activity along the west coasts of Europe and North America: Algorithm formulation, reanalysis uncertainty and link to atmospheric circulation patterns, *Clim. Dyn.*, *48*, 2771–2795.

Cassou, C., L. Terray, J. W. Hurrell, and C. Deser (2004), North Atlantic winter climate regimes: Spatial asymmetry, stationarity with time, and oceanic forcing, *J. Clim.*, *17*, 1055–1068.

Cheng, X., and J. M. Wallace (1993), Cluster analysis of the Northern Hemisphere wintertime 500-hPa height field: Spatial patterns, *J. Atmos. Sci.*, *50*(16), 2674–2696.

Christensen, J. H., et al. (2013), Climate phenomena and their relevance for future regional climate change, in *Climate Change 2013: The Physical Science Basis. Contribution of Working Group I to the Fifth Assessment Report of the Intergovernmental Panel on Climate Change*, edited by T. F. Stocker et al., pp. 1217–1308, Cambridge Univ. Press, Cambridge, U. K.

Cohen, J., et al. (2014), Recent Arctic amplification and extreme mid-latitude weather, *Nat. Geosci.*, *7*, 627–637.

Compo, G. P., et al. (2011), The twentieth century reanalysis project, *Q. J. R. Meteorol. Soc.*, *137*, 1–28.

Coumou, D., and S. Rahmstorf (2012), A decade of weather extremes, *Nat. Clim. Change*, *2*, 491–496.

Croci-Maspoli, M., C. Schwierz, and H. C. Davies (2007), Atmospheric blocking: Space-time links to the NAO and PNA, *Clim. Dyn.*, *29*, 713–725.

Dacre, H. F., P. A. Clark, O. Martinez-Alvarado, M. A. Stringer, and D. A. Lavers (2015), How do atmospheric rivers form?, *Bull. Am. Meteorol. Soc.*, *96*, 1243–1255.

Davini, P., C. Cagnazzo, R. Neale, and J. Tribbia (2012), Coupling between Greenland blocking and the North Atlantic Oscillation pattern, *Geophys. Res. Lett.*, *39*, L14701, doi:10.1029/2012GL052315.

Davini, P., J. von Hardenberg, and S. Corti (2015), Tropical origin for the impacts of the Atlantic Multidecadal Variability on the Euro-Atlantic climate, *Environ. Res. Lett.*, *10*(9), 094010, doi:10.1088/1748-9326/10/9/094010.

Dee, D. P., et al. (2011), The ERA-Interim reanalysis: Configuration and performance of the data assimilation system, *Q. J. R. Meteorol. Soc.*, *137*, 553–597.

Dommenget, D., and M. Latif (2002), A cautionary note on the interpretation of EOFs, *J. Clim.*, *15*, 216–225.

Fleig, A. K., L. M. Tallaksen, P. James, H. Hisdal, and K. Stahl (2014), Attribution of European precipitation and temperature trends to changes in circulation types, *Hydrol. Earth Syst. Sci. Discuss.*, *11*, 12,799–12,831.

Francis, J. A., and S. J. Vavrus (2012), Evidence linking Arctic amplification to extreme weather in mid-latitudes, *Geophys. Res. Lett.*, *39*, L06801, doi:10.1029/2012GL051000.

Gao, Y., J. Lu, and L. R. Leung (2016), Uncertainties in projecting future changes in atmospheric rivers and their impacts on heavy precipitation over Europe, *J. Clim.*, *29*, 6711–6726.

Gastineau, G., and C. Frankignoul (2015), Influence of the North Atlantic SST variability on the atmospheric circulation during the twentieth century, *J. Clim.*, *28*, 1396–1416.

Gastineau, G., F. D'Andrea, and C. Frankignoul (2013), Atmospheric response to the North Atlantic Ocean variability on seasonal to decadal time scales, *Clim. Dyn.*, *40*, 2311–2330.

Gimeno, L., R. Nieto, M. Vazquez, and D. A. Lavers (2014), Atmospheric rivers: A mini-review, *Front. Earth Sci.*, *2*, 2, doi:10.3389/feart.2014.00002.

Gulev, S. K., M. Latif, N. Keenlyside, W. Park, and K. P. Koltermann (2013), North Atlantic Ocean control on surface heat flux on multidecadal timescales, *Nature*, *499*, 464–468.

Häkkinen, S., P. B. Rhines, and D. L. Worthen (2011), Atmospheric blocking and Atlantic multidecadal ocean variability, *Science*, *334*, 655–659.

Haylock, M. R., N. Hofstra, A. M. G. Klein Tank, E. J. Klok, P. D. Jones, and M. New (2008), A European daily high-resolution gridded dataset of surface temperature and precipitation, *J. Geophys. Res.*, *113*, D20119, doi:10.1029/2008JD010201.

Huffman, G. J., R. F. Adler, D. T. Bolvin, and G. Gu (2009), Improving the global precipitation record: GPCP version 2.1, *Geophys. Res. Lett.*, *36*, L17808, doi:10.1029/2009GL040000.

Huntingford, C., et al. (2014), Potential influences on the United Kingdom's floods of winter 2013/14, *Nat. Clim. Change*, *4*, 769–777.

Hurrell, J. W. (1995), Decadal trends in the North Atlantic Oscillation and relationships to regional temperature and precipitation, *Science*, *269*, 676–679.

Hurrell, J. W., and C. Deser (2009), North Atlantic climate variability: The role of the North Atlantic Oscillation, *J. Mar. Syst.*, *78*, 28–41.

IPCC (2013), Summary for policymakers, in *Climate Change 2013: The Physical Science Basis. Contribution of Working Group I to the Fifth Assessment Report of the Intergovernmental Panel on Climate Change*, edited by T. F. Stocker et al., pp. 3–29, Cambridge Univ. Press, Cambridge, U. K.

Keenlyside, N., and N.-E. Omrani (2014), Has a warm North Atlantic contributed to recent European cold winters?, *Environ. Res. Lett.*, *9*, 061001, doi:10.1088/1748-9326/9/6/061001.

Kendon, M., and M. McCarthy (2015), The UK's wet and stormy winter of 2013/2014, *Weather*, *70*(2), 40–47.

KleinTank, A. M. G., and G. P. Können (2003), Trends in indices of daily temperature and precipitation extremes in Europe, *J. Clim.*, *16*, 3665–3680.

Lavers, D. A., and G. Villarini (2013), The nexus between atmospheric rivers and extreme precipitation across Europe, *Geophys. Res. Lett.*, *40*, 3259–3264, doi:10.1002/grl.50636.

Lavers, D. A., R. P. Allan, E. F. Wood, G. Villarini, D. J. Brayshaw, and A. J. Wade (2011), Winter floods in Britain are connected to atmospheric rivers, *Geophys. Res. Lett.*, *38*, L23803, doi:10.1029/2011GL049783.

Lavers, D. A., G. Villarini, R. P. Allan, E. F. Wood, and A. J. Wade (2012), The detection of atmospheric rivers in atmospheric reanalyses and their links to British winter floods and the large-scale climatic circulation, *J. Geophys. Res.*, *117*, D20106, doi:10.1029/2012JD018027.

Luo, D., Y. Yao, and A. Dai (2015), Decadal relationship between European blocking and the North Atlantic Oscillation during 1978–2011. Part I: Atlantic conditions, *J. Atmos. Sci.*, *72*, 1152–1173.

Macdonald, N. (2014), Millennial scale variability in high magnitude flooding across Britain, *Hydrol. Earth Syst. Sci.*, *11*, 10,157–10,178.

Maidens, A., A. Arribas, A. A. Scaife, C. MacLachlan, D. Peterson, and J. Knight (2013), The influence of surface forcings on prediction of the North Atlantic Oscillation regime of winter 2010/11, *Mon. Weather Rev.*, *141*, 3801–3813.

Moberg, A., et al. (2006), Indices for daily temperature and precipitation extremes in Europe analyzed for the period 1901–2000, *J. Geophys. Res.*, *111*, D22106, doi:10.1029/2006JD007103.

Pall, P., T. Aina, D. A. Stone, P. A. Stott, T. Nozawa, A. G. J. Hilberts, D. Lohmann, and M. R. Allen (2011), Anthropogenic greenhouse gas contribution to flood risk in England and Wales in autumn 2000, *Nature*, *470*, 382–385.

Peings, Y., and G. Magnusdottir (2014), Forcing of the wintertime atmospheric circulation by the multidecadal fluctuations of the North Atlantic ocean, *Environ. Res. Lett.*, *9*, 061001, doi:10.1088/1748-9326/9/3/034018.

Rayner, N. A., D. E. Parker, E. B. Horton, C. K. Folland, L. V. Alexander, D. P. Rowell, E. C. Kent, and A. Kaplan (2003), Global analyses of sea surface temperature, sea ice, and night marine air temperature since the late nineteenth century, *J. Geophys. Res.*, *108*(D14), 4407, doi:10.1029/2002JD002670.

Rex, D. F. (1950), Blocking action in the middle troposphere upon regional climate: I. An aerological study of blocking, *Tellus*, *2*, 196–211.

Reynolds, R. W., N. A. Rayner, T. M. Smith, D. C. Stokes, and W. Wang (2002), An improved in situ and satellite SST analysis for climate, *J. Clim.*, *15*, 1609–1625.

Scaife, A. A., C. K. Folland, L. V. Alexander, A. Moberg, and J. R. Knight (2008), European climate extremes and the North Atlantic Oscillation, *J. Clim.*, *21*, 72–83.

Scherrer, S. C., M. Croci-Maspoli, C. Schwierz, and C. Appenzeller (2006), Two-dimensional indices of atmospheric blocking and their statistical relationship with winter climate patterns in the Euro-Atlantic region, *Int. J. Climatol.*, *26*, 233–249.

Schneider, U., A. Becker, P. Finger, A. Meyer-Christoffer, M. Ziese, and B. Rudolf (2014), GPCC's new land surface precipitation climatology based on quality-controlled in situ data and its role in quantifying the global water cycle, *Theor. Appl. Climatol.*, *115*, 1–15.

Screen, J. A., and I. Simmonds (2014), Amplified mid-latitude planetary waves favour particular regional weather extremes, *Nat. Clim. Change*, *4*, 704–709.

Spinoni, J., G. Naumann, J. V. Vogt, and P. Barbosa (2015), The biggest drought events in Europe from 1950 to 2012, *J. Hydrol.*, *3*, 509–524, doi:10.1016/j.ejrh.2015.01001.

Uppala, S. M., et al. (2005), The ERA-40 re-analysis, *Q. J. R. Meteorol. Soc.*, *131*, 2961–3012.

Vautard, R. (1990), Multiple weather regimes over the North Atlantic: Analysis of precursors and successors, *Mon. Weather Rev.*, *118*, 2056–2081.

Ward, J. (1963), Hierarchical grouping to optimize an objective function, *J. Am. Stat. Assoc.*, *58*, 236–244.

Woollings, T., and M. Blackburn (2012), The North Atlantic jet stream under climate change and its relation to the NAO and EA patterns, *J. Clim.*, *25*, 886–902.

Woollings, T., B. Hoskins, M. Blackburn, and P. Berrisford (2008), A new Rossby wave-breaking interpretation of the North Atlantic Oscillation, *J. Atmos. Sci.*, *65*, 609–626.

Woollings, T., A. Hannachi, and B. Hoskins (2010), Variability of the North Atlantic eddy-driven jet stream, *Q. J. R. Meteorol. Soc.*, *136*, 856–868.

Xie, P., and P. A. Arkin (1996), Analyses of global monthly precipitation using gauge observations, satellite estimates, and numerical model predictions, *J. Clim.*, *9*, 840–858.

Zhu, Y., and R. Newell (1994), Atmospheric rivers and bombs, *Geophys. Res. Lett.*, *21*(18), 1999–2002.

Zolina, O., C. Simmer, A. Kapala, and S. Gulev (2005), On the robustness of the estimates of centennial-scale variability in heavy precipitation from station data over Europe, *Geophys. Res. Lett.*, *32*, L14707, doi:10.1029/2005GL023,231.

Zolina, O., C. Simmer, K. Belyaev, A. Kapala, and S. Gulev (2009), Improving estimates of heavy and extreme precipitation using daily records from European rain gauges, *J. Hydrometeorol.*, *10*, 701–716.

Zolina, O., C. Simmer, K. Belyaev, S. K. Gulev, and P. Koltermann (2013), Changes in the duration of European wet and dry spells during the last 60 years, *J. Clim.*, *26*, 2022–2047.

Zolina, O., C. Simmer, A. Kapala, P. Shabanov, P. Becker, H. Mächel, S. Gulev, and P. Groisman (2014), Precipitation variability and extremes in central Europe: New view from STAMMEX results, *Bull. Am. Meteorol. Soc.*, *95*, 995–1002.

Supporting Information for "Emerging European winter precipitation pattern in recent decades linked to North Atlantic circulation changes"

DOI: 10.1002/

Caroline C. Ummenhofer,[1] Hyodae Seo[1], Young-Oh Kwon[1], Rhys Parfitt[1], Swen Brands[2], Terrence M. Joyce[1]

Corresponding author: C. C. Ummenhofer, Department of Physical Oceanography, Woods Hole Oceanographic Institution, Woods Hole, MA, USA. (cummenhofer@whoi.edu)

[1]Department of Physical Oceanography, Woods Hole Oceanographic Institution, Woods Hole, Massachusetts, USA

[2]MeteoGalicia - Xunta de Galicia, Consellería de Medio Ambiente e Ordenación do Territorio, Santiago de Compostela, Spain

Contents of this file

Text S1. European precipitation

Precipitation across Europe has sustained considerable annual trends over the past century [*IPCC*, 2013]: central, western, and northern Europe have become significantly wetter for the period 1901–2010, while southern Europe (including the Iberian Peninsula, much of Italy and the Balkan States) has sustained significant drying over the same period [*IPCC*, 2013]. These broad-scale precipitation changes are also borne out during the cool season, with wintertime precipitation totals north of 40°N increasing significantly by approximately 12% over the period 1901–2000 [*Moberg et al.*, 2006]. The intensity and frequency of European extreme precipitation has also increased over recent decades, especially in winter [*Christensen et al.*, 2013]. Additionally, for the cool-season 1950–2009, *Zolina et al.* [2013] found the duration of wet spells to have increased (decreased) in northern, central, and eastern (southern) Europe by 15–20%. This pattern (i.e., wetter north, drier south) across Europe has previously been associated with the NAO [e.g., *Hurrell*, 1995] and AMO [*Alexander et al.*, 2014].

According to the Summary for Policymakers from the Intergovernmental Panel for Climate Change (IPCC) Assessment Report 5 (AR5), confidence in precipitation change over the mid-latitude land areas of the Northern Hemisphere is medium for the period 1901–1950 and high post-1951 [*IPCC*, 2013]. The limited availability and spatial coverage of long-term high-quality daily European precipitation station data prior to the 1950s makes it difficult to assess long-term trends in precipitation extremes [e.g., *KleinTank and Können*, 2003; *Zolina et al.*, 2005, 2014], compared to mean precipitation changes [*Zolina et al.*, 2009]. Our study therefore focuses on *seasonal precipitation totals*, rather than *daily extremes*, and on year-to-year variations for wintertime precipitation averages, rather than long-term trends. The latter are particularly sensitive to the endpoints of a time-series, while interannual variability of wintertime precipitation totals as evaluated here is less affected by any individual values near the endpoints of the time-series.

Here we use the Global Precipitation Climatology Centre v6 product (GPCC; 1901–2010). A detailed comparison between GPCC's precipitation product and a variety of precipitation climatologies derived from satellites, station observations, and model re-analyses by the European Center for Medium range Weather Forecasting (ECMWF), ie. ERA-40 and ERA-interim [*Uppala et al.*, 2005; *Dee et al.*, 2011], is provided by *Schneider et al.* [2014]. Over the common analysis period 1958–2001, they found large differences (in excess of 50 mm/yr) between the GPCC climatology and ERA-40, extending in a band from the British Isles and the Iberian Peninsula over central Europe eastward until 100°E, with GPCC consistently wetter than ERA-40 [*Schneider et al.*, 2014]. For the period 1979–2010, the differences between GPCC and ERA-interim over Europe were generally smaller than for ERA-40. Comparing the Global Precipitation Climatology Project (GPCP) v2.2 product [*Huffman et al.*, 2009] with GPCC for the period 1988–2010, differences in the precipitation climatology are consistently below 50 mm/yr across Europe [*Schneider et al.*, 2014].

The dominant wintertime precipitation regimes identified in the present study are compared for two different precipitation products, namely GPCC v6 [*Schneider et al.*, 2014] and the daily gridded observational product from the ENSEMBLES project [E-OBS v15.0; *Haylock et al.*, 2008], both at 0.5° horizontal resolution and for the period 1950–2010

(Fig. S1). The precipitation anomalies in the five different clusters are very similar between the two products and consistent with those shown for the longer period in Fig. 1a.

Text S2. Data and methods

Atmospheric blocking

A day is defined as being blocked based on the meridional gradient of the daily geopotential height at 500hPa (Z500) following *Scherrer et al.* [2006] and *Häkkinen et al.* [2011]. On each day, at a given location, the meridional gradients are calculated against the locations 15° north and south, respectively:

$$\triangle Z500_S = \frac{Z500(x_0, y_0) - Z500(x_0, y_S)}{y_0 - y_S} \tag{1}$$

$$\triangle Z500_N = \frac{Z500(x_0, y_N) - Z500(x_0, y_0)}{y_N - y_0} \tag{2}$$

where x_0 and y_0 are the reference longitude and latitude, respectively, while $y_S = y_0 - 15$ and $y_N = y_0 + 15$. When there is blocking, we expect the gradient to the south to be reversed ($\triangle Z500_S > 0$) and the gradient to the north to be steeper than usual ($\triangle Z500_N < -10 m/°latitude$). Once these two criteria are met on any given day and location, an instantaneous block is identified. If five or more consecutive days of instantaneous blocking are found at a location, then those days are identified as the blocked days. No further criterion to account for additional spatial and temporal coherences [*Barnes et al.*, 2012] is considered. The index captures Rossby wave breaking activity and resulting cutoff anticyclones over Europe lasting longer than 5 days [e.g., *Woollings et al.*, 2008; *Davini* *et al.*, 2012]: as such the index identifies events in the subtropical latitudes that only affect the jet stream moderately, high-latitude events that dislocate the jet equatorward, as well as mid-latitude blocking events, as originally defined by *Rex* [1950]. This spatial blocking variability is also closely associated with the tri-modal variability of the North Atlantic eddy-driven jet [*Woollings et al.*, 2010].

Vertically integrated water-vapor transport and atmospheric rivers

The algorithm used here for the detection and tracking of atmospheric rivers (ARs) operates on the intensity (IVT, in kg^{-1} m^{-1} s^{-1}) and direction (D, in degrees) of the vertically integrated water vapor transport (IVT) obtained from six-hourly instantaneous reanalysis data [e.g., *Lavers et al.*, 2012]:

$$IVT = \sqrt{IVT_U{}^2 + IVT_V{}^2} \tag{3}$$

$$D = atan2(\frac{IVT_U}{IVT}, \frac{IVT_V}{IVT})\frac{180}{\pi} + 180 \tag{4}$$

where IVT_U and IVT_V are the zonal and meridional components of the vertically integrated water vapor flux, respectively. The $atan2$ function returns the four-quadrant inverse tangent ranging in between $-\pi$ and π, which is then transformed to degree values ranging in between 0° and 360°. For IVT_U and IVT_V, the two components were calculated upon the zonal and meridional wind components and the specific humidity at 15 pressure levels between 1000 and 300 hPa.

After post-processing the reanalysis data in this way, eight target regions were defined along the west coast of Europe, including north-western Africa (Fig. S2). If the IVT in a given region is considered "anomalously strong", the algorithm is activated and essentially "crawls" upstream guided by both the direction and maximum intensity of the flow until the intensity is too weak to be considered anomalously strong. What is actually "anomalously strong" is defined by two types of percentile thresholds; one applied at the grid-boxes defining the target regions ("detection percentile", Pd) and the other along the track identified by the algorithm ("tracking percentile", Pt). Note that Pd and Pt are not necessarily identical. Rather, six distinct combinations of the two parameters were used to assess the method-related uncertainty of the results [e.g., Fig. S7b,d,f; see also *Brands et al.*, 2017].

If the tracked AR structure is longer than 3000 km (the statistics derived from 2000 km are in close agreement), then the target region is assumed to be affected by an AR at this point in time. The six-hourly AR occurrences are summed for each JFM season forming a year-to-year time series of wintertime AR counts for that region during the period 1901–2010. A schematic description of the algorithm is provided in Fig. S3 and the full details are given in *Brands et al.* [2017]. Note that the performance of the algorithm can be visually judged by consulting the *Atmospheric River Archive* at http://www.meteo.unican.es/atmospheric-rivers, a web portal for AR events in Europe and western North America, that covers the period 1900–2014. The binary AR occurrence/absence time series are also publicly available from this source.

Statistical methods

In addition to anomaly maps of precipitation for the different clusters, associated anomalies in atmospheric/oceanic fields helped interpret dominant processes resulting in recurring precipitation patterns. A two-tailed Student's t-test was used to determine the significance of the spatial anomaly fields (Figs. 1–2, S1, S4–S7). At each grid point, it estimates the statistical significance at which the composite mean in any one cluster is distinguishable from the mean of all years.

A Monte Carlo or boot-strapping method was employed to assess variations in the frequency of occurrence of individual clusters over time. In particular, it was determined how many winters in each decade were categorized to fall into each cluster, shown for 20-yr sliding windows in Figs. 3 and S8. To determine whether the number of winters in a certain cluster were unusual in a decade, we randomly selected ten years and determined the frequency of occurrence for each cluster. This was repeated 10,000 times to obtain an expected distribution of frequency of occurrence per decade for each cluster. Whenever the actual frequency of occurrence for a cluster lay above or below the 97.5% or 2.5% level, respectively, a decade was highlighted as having significantly more/fewer events of that particular cluster than expected purely by chance alone at the 5% significance level.

To test whether climatic conditions during the period 1981–2010 differed significantly from conditions during the former period (1951–1980), we used a Monte Carlo bootstrapping method. For each of the variables, we randomly select two sets of 30 years from the full 60-yr record (1951–2010), create a time-average of the climatic field for each set of 30 years, and calculate the difference between the two fields. This process is repeated

1,000 times. The resultant 1,000 difference fields represent an expected distribution of difference fields for a random selection of any two sets of 30 years. At each gridpoint, we then determine whether the actual observed difference between the period 1981–2010 and the earlier period 1951–1980 lies outside the 1% and 99% confidence levels. Fig. 4 indicates where the actual observed differences in the climate fields lie outside the expected difference distributions and thus differs significantly between the two periods.

Text S3. Links to regional circulation for precipitation patterns A–C

Pattern A is characterized by a weakened meridional pressure gradient, reduced westerly flow across northern Europe (north of 45°N; Fig. S5a), enhanced blocking activity over Greenland, the British Isles, and Scandinavia, and reduced storm-track activity over the British Isles (Fig. S5b,c). The subpolar gyre (north of 55°N) is warm (Fig. S5d). For the 2005/06 European winter, one of the winters in this cluster (Table S1), *Croci-Maspoli and Davies* [2009] argued that the warm upstream SST anomalies over the North Atlantic, rather than the negative NAO conditions, were instrumental in setting up enhanced blocking conditions to the west of the European continent. This is in line with the circulation and oceanic conditions associated with pattern A here. Pattern B broadly exhibits circulation anomalies of the opposite sign to A: i.e., B is characterized by a strengthened meridional pressure gradient with enhanced westerly flow over Europe north of 40°N, stronger storm-track activity over the British Isles, and weaker blocking activity over the British Isles (Fig. S5). Results are consistent for the shorter period 1979–2010 with improved data coverage and using the ERA-interim reanalysis product (Fig. S6).

The anomalous IVT and numbers of AR occurrence for clusters A–C are shown in Fig. S7. The IVT anomalies and AR counts are consistent with the corresponding precipitation patterns with dry conditions in northern Europe and wet conditions in western/central Europe for clusters A and B, respectively: cluster A exhibits reduced IVT over the British Isles and northern Europe, with anomalously few AR events reaching the British Isles and Norway (Fig. S7a,b); in contrast, in cluster B, France is affected by significantly more AR events, along with anomalous wet IVT anomalies for western and central Europe (Fig. S7c,d). Years in cluster C exhibit a significant reduction (increase) in IVT over the British Isles and northern Europe (southern and central Europe), resulting in fewer (more) AR events for the British Isles and Norway (Iberian Peninsula and France; Fig. S7e,f).

The frequency of the dominant JFM precipitation patterns described here varied over time. The number of events, i.e. how often a winter was classified as a particular pattern A–C in each decade, is shown in Fig. S8 for the period 1901–2010. Multidecadal variations in the frequency of occurrence of the different clusters are apparent, although the anomalies are statistically significant only in limited time periods. Pattern A occurred on average 1–2 times per decade for much of the 20th Century. However, in the late 1950s and early 1960s, this pattern was unusually common with 3 or more events per decade (Fig. S8), consistent with more frequent drought conditions in northern and eastern Europe during the 1950s and 1960s [*Spinoni et al.*, 2015]. Pattern B, was unusually common in the 1920s, occurring 4–5 times per decade, potentially accounting for more frequent flooding in the UK [*Macdonald*, 2014]. In contrast, it occurred twice or less per decade during the 1940s. Pattern C was uncommon during positive NAO phases (e.g., in the 1920s), while it occurred significantly more frequently (3–4 times per decade) around 1970 when the NAO was in a low phase.

References

Alexander, M. A., K. H. Kilbourne, and J. A. Nye (2014), Climate variability during warm and cold phases of the Atlantic Multidecadal Oscillation (AMO) 1871-2008, *Journal of Marine Systems*, *133*, 14–26.

Barnes, E. A., J. Slingo, and T. Woollings (2012), A methodology for the comparison of blocking climatologies across indices, models and climate scenarios, *Climate Dynamics*, *38*, 24672481.

Brands, S., J. M. Gutierrez, and D. San Martin (2017), Twentieth-century atmospheric river activity along the west coasts of Europe and North America: Algorithm formulation, reanalysis uncertainty and link to atmospheric circulation patterns, *Climate Dynamics*, *48*, 2771–2795.

Christensen, J. H., K. Krishna Kumar, E. Aldrian, S.-I. An, I. F. A. Cavalcanti, M. de Castro, W. Dong, P. Goswami, A. Hall, J. K. Kanyanga, A. Kitoh, J. Kossin, N.-C. Lau, J. Renwick, D. B. Stephenson, S.-P. Xie, and T. Zhou (2013), Climate phenomena and their relevance for future regional climate change, in *Climate Change 2013: The Physical Science Basis. Contribution of Working Group I to the Fifth Assessment Report of the Intergovernmental Panel on Climate Change*, edited by T. F. Stocker, D. Qin, G.-K. Plattner, M. Tignor, S. K. Allen, J. Boschung, A. Nauels, Y. Xia, V. Bex, and P. M. Midgley, pp. 1217–1308, Cambridge University Press, Cambridge, UK.

Croci-Maspoli, M., and H. C. Davies (2009), Key dynamical features of the 2005/06 European winter, *Monthly Weather Review*, *137*, 664–678.

Davini, P., C. Cagnazzo, R. Neale, and J. Tribbia (2012), Coupling between Greenland blocking and the North Atlantic Oscillation pattern, *Geophysical Research Letters*, *39*, doi:10.1029/2012GL052,315.

Dee, D. P., S. M. Uppala, and Coauthors (2011), The ERA-Interim reanalysis: configuration and performance of the data assimilation system, *Quaterly Journal of the Royal Meteorological Society*, *137*, 553–597.

Häkkinen, S., P. B. Rhines, and D. L. Worthen (2011), Atmospheric blocking and Atlantic multidecadal ocean variability, *Science*, *334*, 655–659.

Haylock, M. R., N. Hofstra, A. M. G. Klein Tank, K. E. J., P. D. Jones, and M. New (2008), A European daily high-resolution gridded dataset of surface temperature and precipitation., *Journal of Geophysical Research*, *113*, doi:10.1029/2008JD010,201.

Huffman, G. J., R. F. Adler, D. T. Bolvin, and G. Gu (2009), Improving the global precipitation record: GPCP version 2.1., *Geophysical Research Letters*, *36*(L17808), doi:10.1029/2009GL040,000.

Hurrell, J. W. (1995), Decadal trends in the North Atlantic Oscillation and relationships to regional temperature and precipitation, *Science*, *269*, 676–679.

IPCC (2013), Summary for policymakers, in *Climate Change 2013: The Physical Science Basis. Contribution of Working Group I to the Fifth Assessment Report of the Intergovernmental Panel on Climate Change*, edited by T. F. Stocker, D. Qin, G.-K. Plattner, M. Tignor, S. K. Allen, J. Boschung, A. Nauels, Y. Xia, V. Bex, and P. M. Midgley, pp. 3–29, Cambridge University Press, Cambridge, UK.

KleinTank, A. M. G., and G. P. Können (2003), Trends in indices of daily temperature and precipitation extremes in Europe, *Journal of Climate*, *16*, 3665–3680.

Lavers, D. A., G. Villarini, R. P. Allan, E. F. Wood, and A. J. Wade (2012), The detection of atmospheric rivers in atmospheric reanalyses and their links to British winter floods and the large-scale climatic circulation, *Journal of Geophysical Research - Atmosphere*, *117*, doi:10.1029/2012JD018,027.

Macdonald, N. (2014), Millennial scale variability in high magnitude flooding across Britain, *Hydrology and Earth System Sciences*, *11*, 10,157–10,178.

Moberg, A., P. D. Jones, D. Lister, A. Walther, M. Brunet, J. Jacobeit, L. V. Alexander, P. M. Della-Marta, J. Luterbacher, P. Yiou, D. Chen, A. M. G. KleinTank, O. Saladie, J. Sigro, E. Aguilar, H. Alexandersson, C. Almaraza, I. Auer, M. Barriendos, M. Begert, H. Bergström, R. Böhm, C. J. Butler, J. Caesar, A. Drebs, D. Founda, F.-W. Gerstengarbe, G. Micela, M. Maugeri, H. Österle, K. Pandzic, M. Petrakis, L. Srnec, R. Tolasz, H. Tuomenvirta, P. C. Werner, H. Linderholm, A. Philipp, H. Wanner, and E. Xoplaki (2006), Indices for daily temperature and precipitation extremes in Europe analyzed for the period 1901-2000, *Journal of Geophysical Research*, *111*(D22106), doi:10.1029/2006JD007,103.

Rex, D. F. (1950), Blocking action in the middle troposphere upon regional climate: I. An aerological study of blocking, *Tellus*, *2*, 196–211.

Scherrer, S. C., M. Croci-Maspoli, C. Schwierz, and C. Appenzeller (2006), Two-dimensional indices of atmospheric blocking and their statistical relationship with winter climate patterns in the Euro-Atlantic region, *International Journal of Climatology*, *26*, 233–249.

Schneider, U., A. Becker, P. Finger, A. Meyer-Christoffer, M. Ziese, and B. Rudolf (2014), GPCC's new land surface precipitation climatology based on quality-controlled in situ data and its role in quantifying the global water cycle, *Theoretical and Applied Climatology*, *115*, 1–15.

Spinoni, J., G. Naumann, J. V. Vogt, and P. Barbosa (2015), The biggest drought events in Europe from 1950 to 2012, *Journal of Hydrology*, p. doi:10.1016/j.ejrh.2015.01.001.

Uppala, S. M., P. W. Kallberg, A. J. Simmons, U. Andrae, V. da Costa Bechtold, M. Fiorino, J. K. Gibson, J. Haseler, A. Hernandez, G. A. Kelly, X. Li, K. Onogi, S. Saarinen, N. Sokka, R. P. Allan, E. Andersson, K. Arpe, M. A. Balmaseda, A. C. M. Beljaars, L. van de Berg, J. Bidlot, N. Bormann, S. Caires, F. Chevallier, A. Dethof, M. Dragosavac, M. Fisher, M. Fuentes, S. Hagemann, E. Holm, B. J. Hoskins, L. Isaksen, P. A. E. M. Janssen, R. Jenne, A. P. McNally, J.-F. Mahfouf, J.-J. Morcrette, N. A. Rayner, R. W. Saunders, P. Simon, A. Sterl, K. E. Trenberth, A. Untch, D. Vasiljevic, P. Viterbo, and J. Woollen (2005), The ERA-40 re-analysis, *Quart. J. Roy. Meteor. Soc.*, *131*, 2961–3012.

Woollings, T., B. Hoskins, M. Blackburn, and P. Berrisford (2008), A new Rossby wave-breaking interpretation of the North Atlantic Oscillation, *Journal of the Atmospheric Sciences*, *65*, 609–626.

Woollings, T., A. Hannachi, and B. Hoskins (2010), Variability of the North Atlantic eddy-driven jet stream, *Quarterly Journal of the Royal Meteorological Society*, *136*, 856–868.

Zolina, O., C. Simmer, A. Kapala, and S. Gulev (2005), On the robustness of the estimates of centennial-scale variability in heavy precipitation from station data over Europe, *Geophysical Research Letters*, *32*(L14707), doi:10.1029/2005GL023,231.

Zolina, O., C. Simmer, K. Belyaev, A. Kapala, and S. Gulev (2009), Improving estimates of heavy and extreme precipitation using daily records from European rain gauges, *Journal of Hydrometeorology*, *10*, 701–716.

Zolina, O., C. Simmer, K. Belyaev, S. K. Gulev, and P. Koltermann (2013), Changes in the duration of European wet and dry spells during the last 60 years, *Journal of Climate*, *26*, 2022–2047.

Zolina, O., C. Simmer, A. Kapala, P. Shabanov, P. Becker, H. Mächel, S. Gulev, and P. Groisman (2014), Precipitation variability and extremes in central Europe: New view from STAMMEX results, *Bulettin of the American Meteorological Society*, *95*, 995–1002.

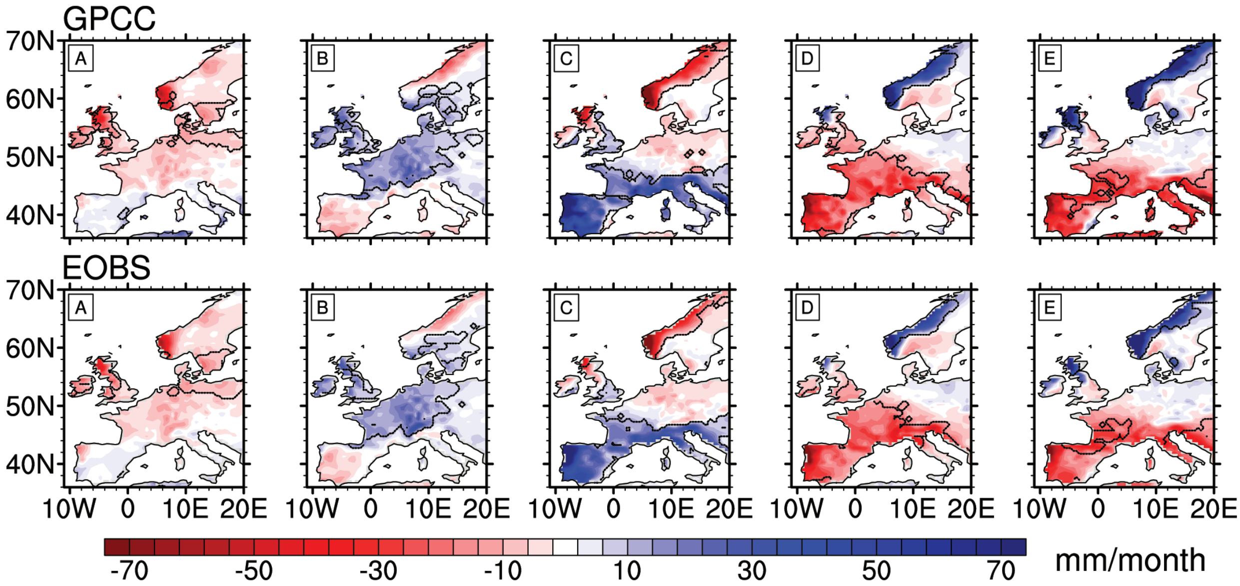

Figure S1. Composite anomalies of precipitation (mm/month) clustered for the European region for GPCC v6 and E-OBS v15.0 gridded precipitation products, both for JFM for the period 1950–2010. The area enclosed by the black contours denotes anomalies that are significant at the 2% significance level as estimated by Student's *t*-test.

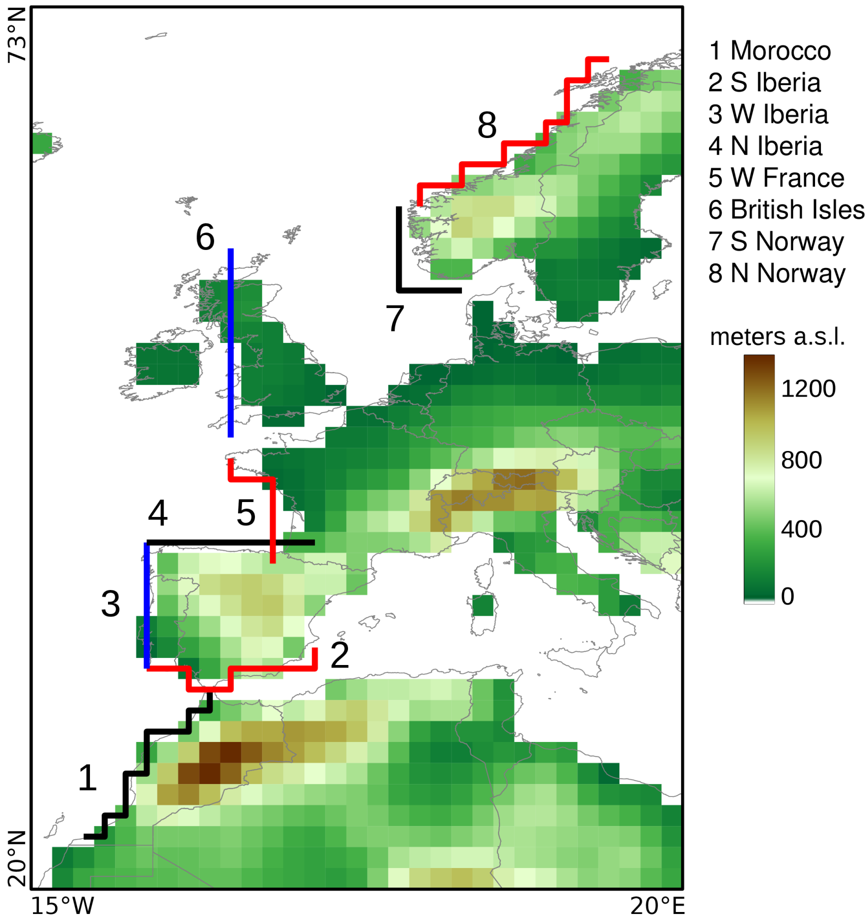

Figure S2. Regions used for the detection of AR events. Adapted from *Brands et al.* [2017].

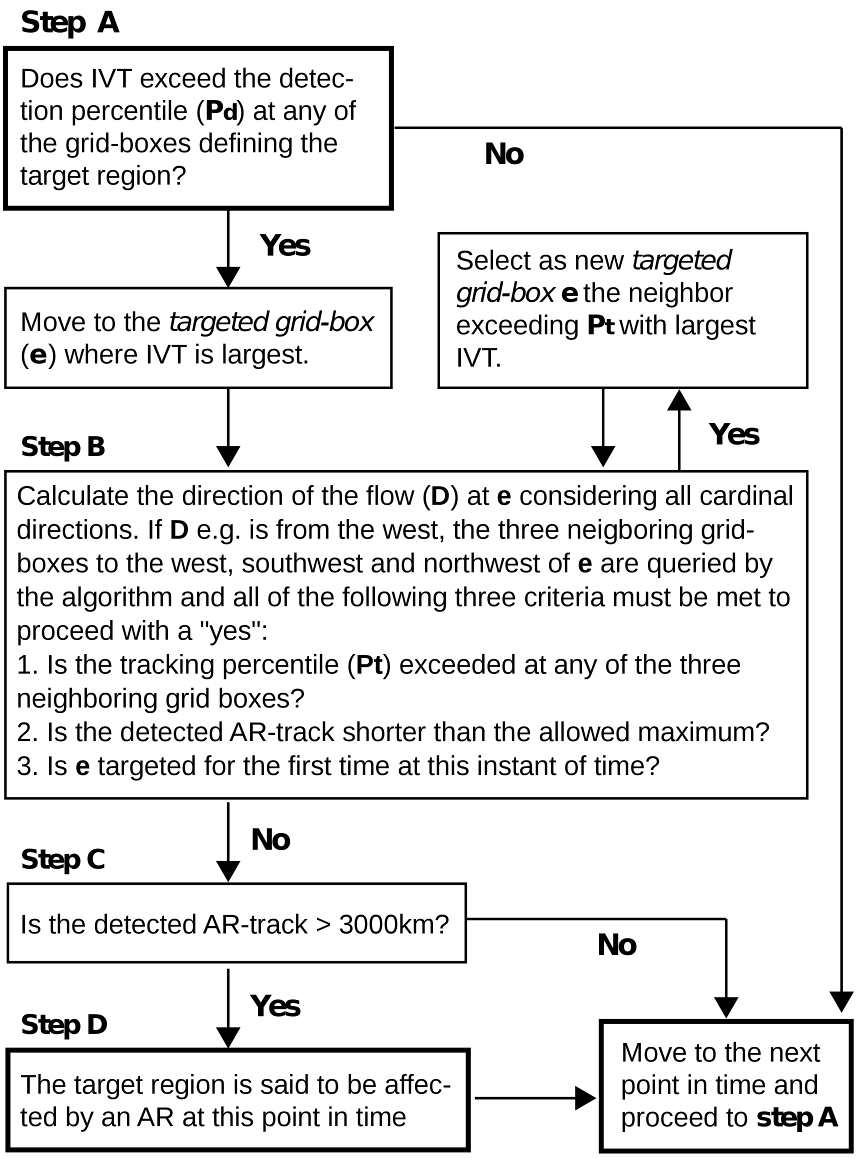

Figure S3. Schematic overview of the algorithm used for the detection and tracking of ARs. Reproduced from *Brands et al.* [2017].

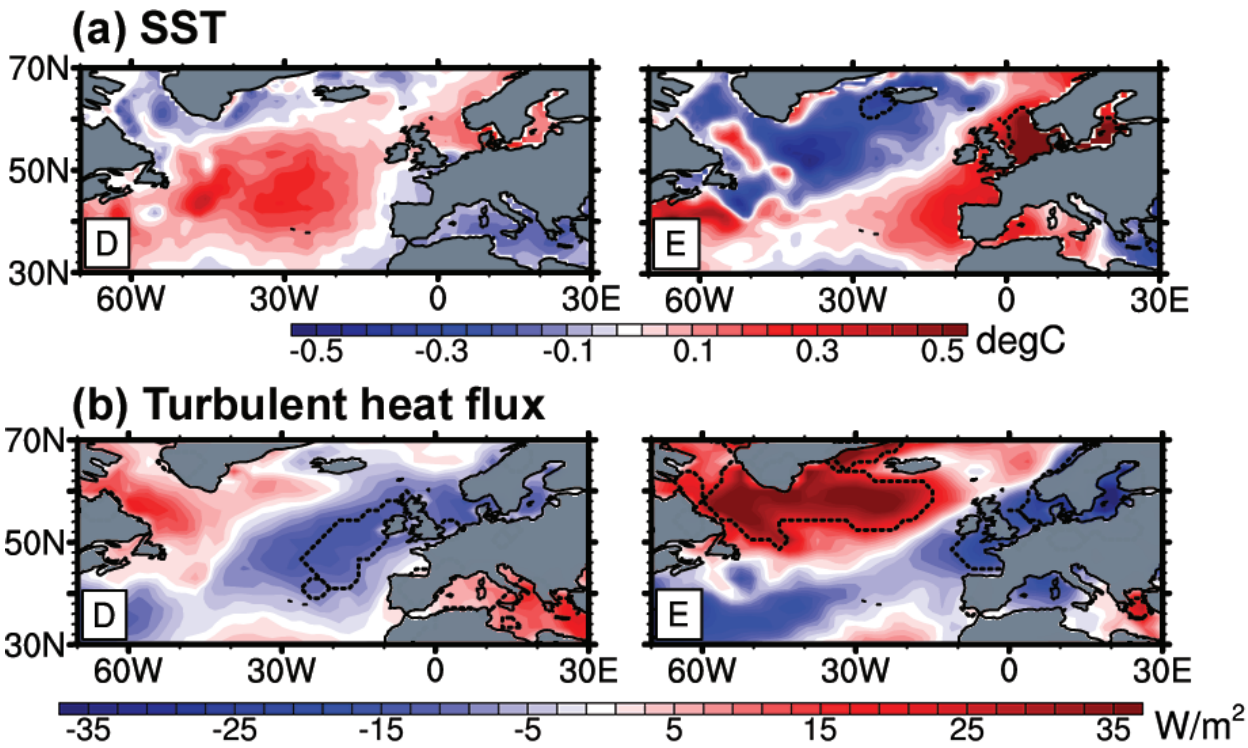

Figure S4. Composite anomalies of (a) SST (°C) and (b) turbulent heat flux, (W/m^2; positive is upward) for JFM for the period 1901–2010 for years in clusters D and E. The area enclosed by the black contours denotes anomalies that are significant at the 2% significance level as estimated by Student's *t*-test.

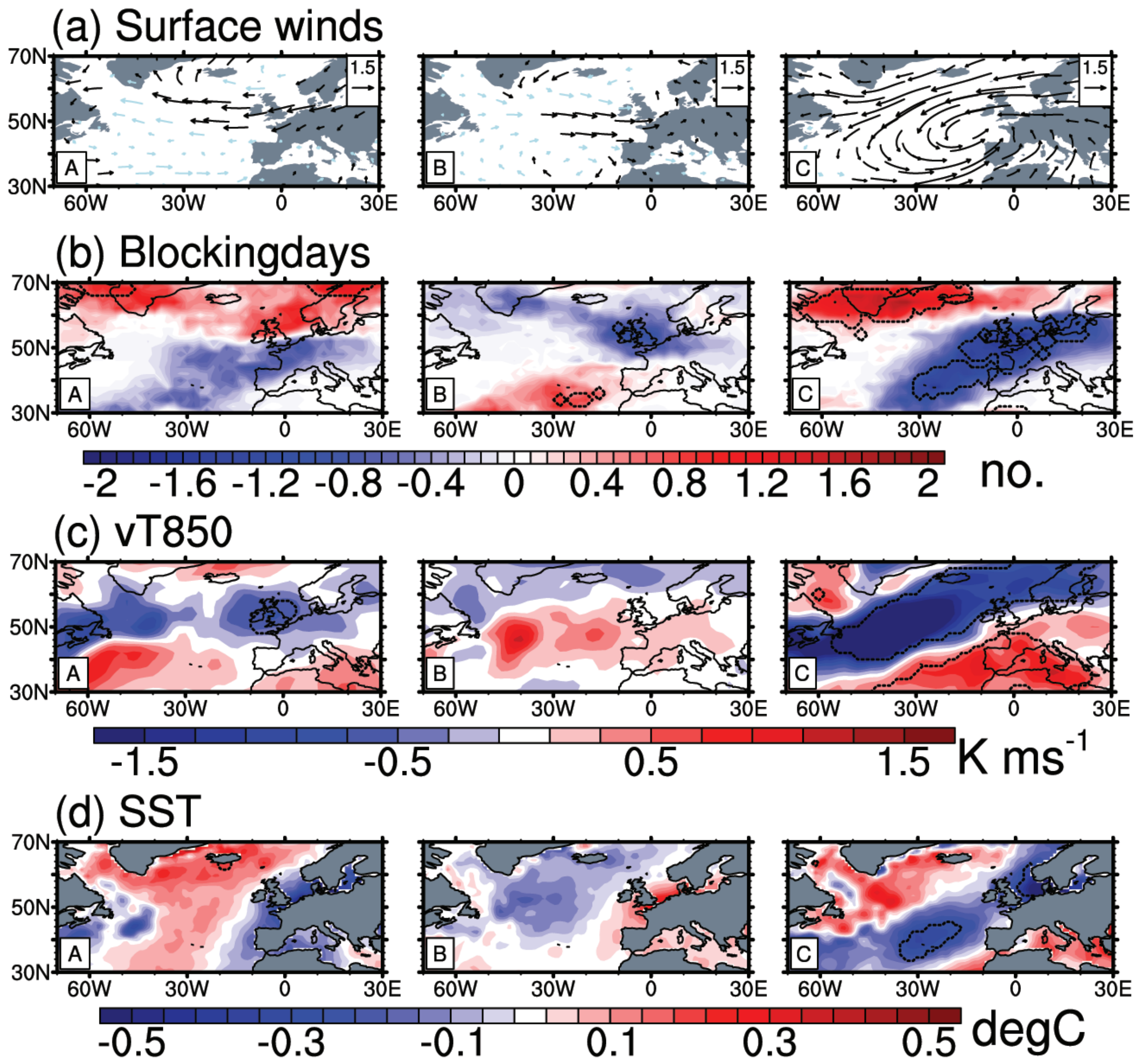

Figure S5. Composite anomalies of (a) surface winds (m/s), (b) number of blocking days per season, (c) 2–6 day band-pass filtered <v'T'> at 850hPa (K m/s), and (d) SST (°C) all for JFM for the period 1901–2010 for years in clusters A to C. The area enclosed by the black contours or black vectors denote anomalies that are significant at the 2% significance level as estimated by Student's *t*-test.

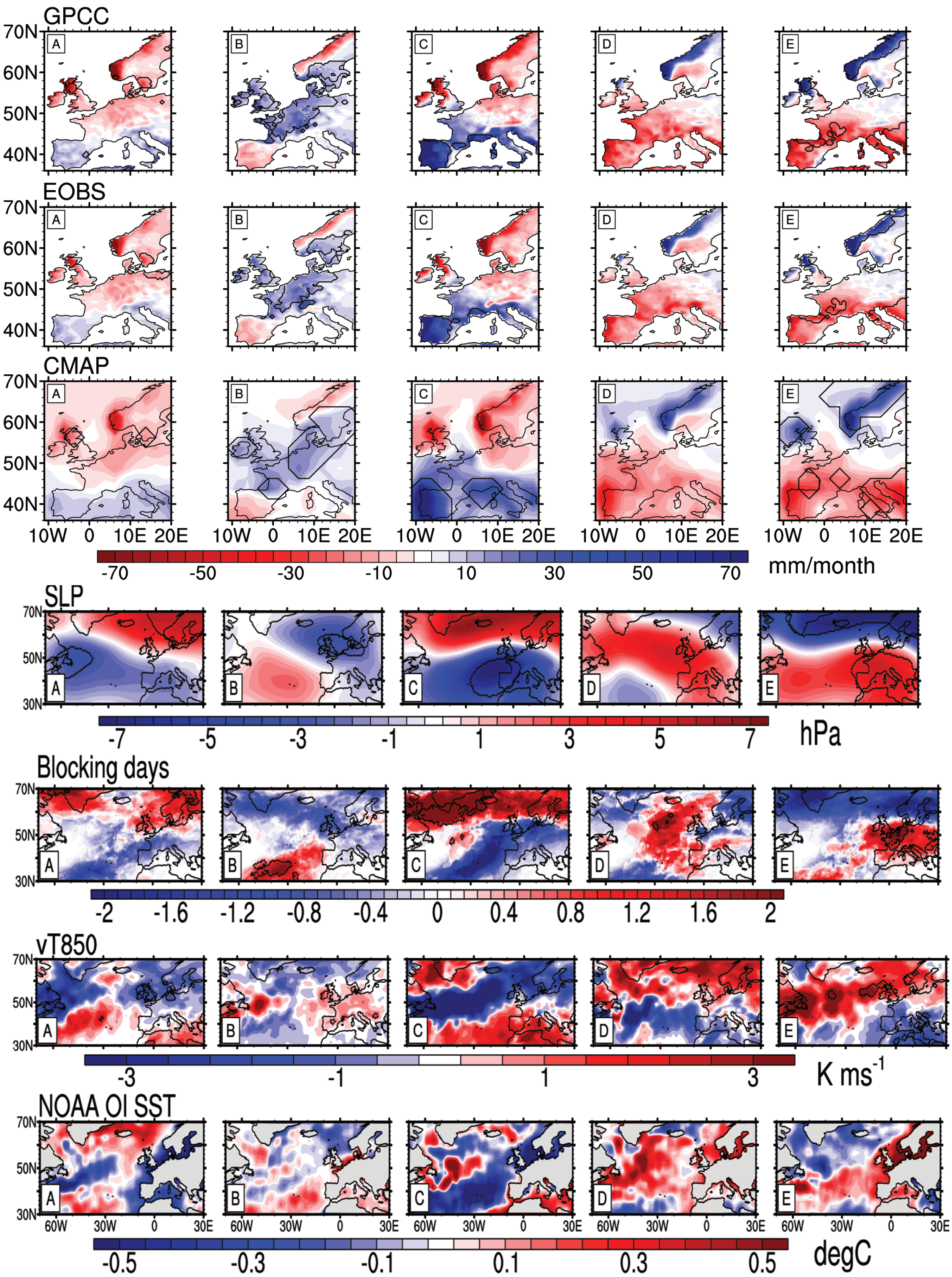
GPCC
EOBS
CMAP
70N
60N
50N
40N
A
B
C
D
E
10W 0 10E 20E
-70 -50 -30 -10 10 30 50 70
mm/month
SLP
30N
-7 -5 -3 -1 1 3 5 7
hPa
Blocking days
-2 -1.6 -1.2 -0.8 -0.4 0 0.4 0.8 1.2 1.6 2
vT850
-3 -1 1 3
K ms-1
NOAA OI SST
60W 30W 0 30E
-0.5 -0.3 -0.1 0.1 0.3 0.5
degC

Figure S6. Composite anomalies during dominant wintertime European precipitation clusters for precipitation (mm/month) for the GPCC v6, E-OBS v15, and CMAP gridded products; ERA-interim SLP (hPa), blocking days, and 2–6 day band-pass filtered <v'T'>; and NOAA Optimum Interpolation SST v2 (°C). All composite anomalies are shown for JFM for the period 1979–2010 (with the exception of NOAA OI SST for the period 1982–2010). The area enclosed by the black contours denotes anomalies that are significant at the 5% significance level as estimated by Student's *t*-test.

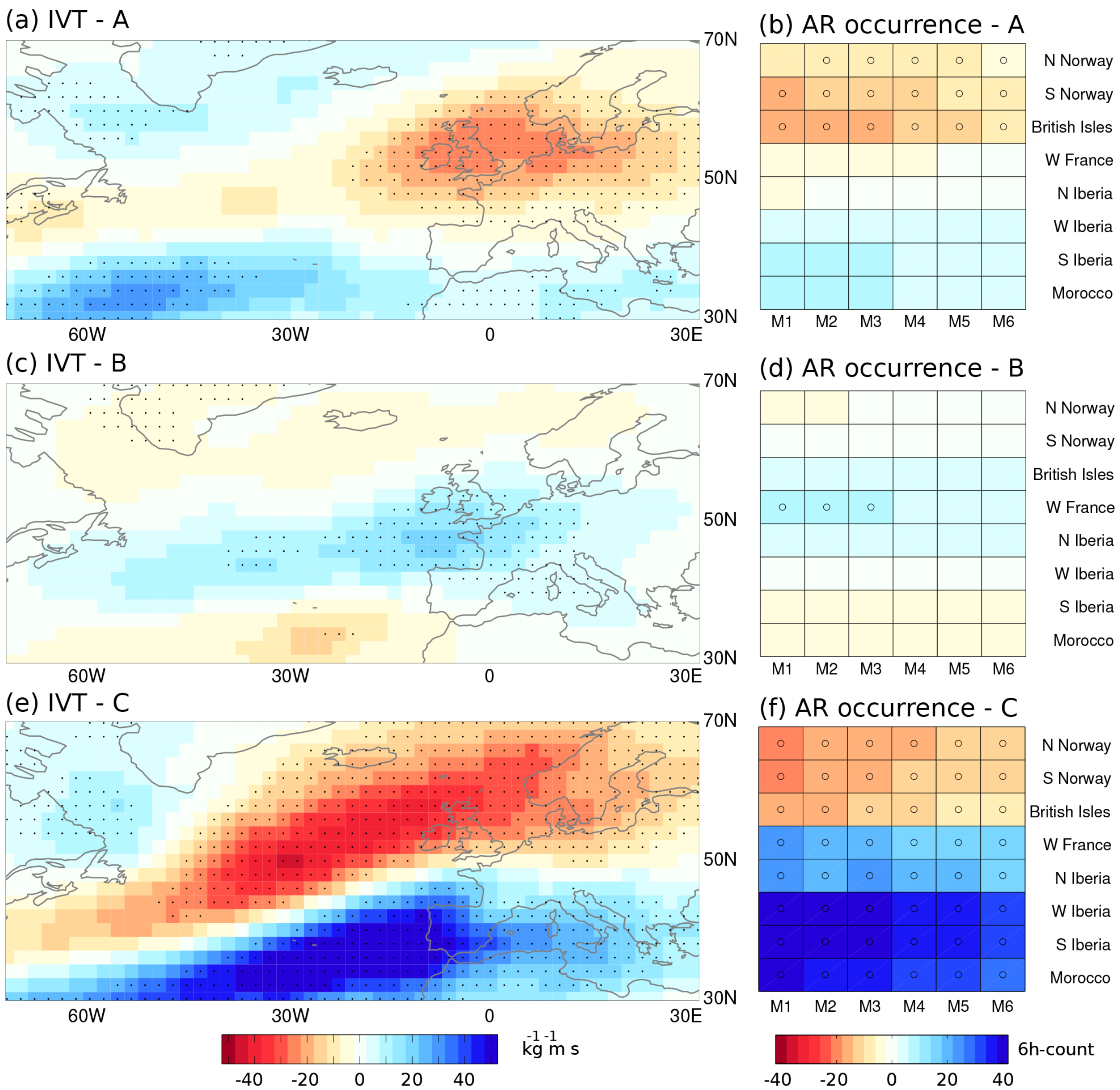

Figure S7. (Left) Composite anomalies of integrated water vapor transport (IVT; kg/m/s) for JFM for the period 1901–2010 for years in clusters A–C. (Right) Count of occurrence of atmospheric river (AR) events for 8 target regions along the eastern Atlantic seaboard. Stippling/circles denote anomalies significant at the 2% significance level as estimated by Student's *t*-test. M1 to M6 represent the six method-modifications of *Brands et al.* [2017] using different percentile-thresholds to define an AR.

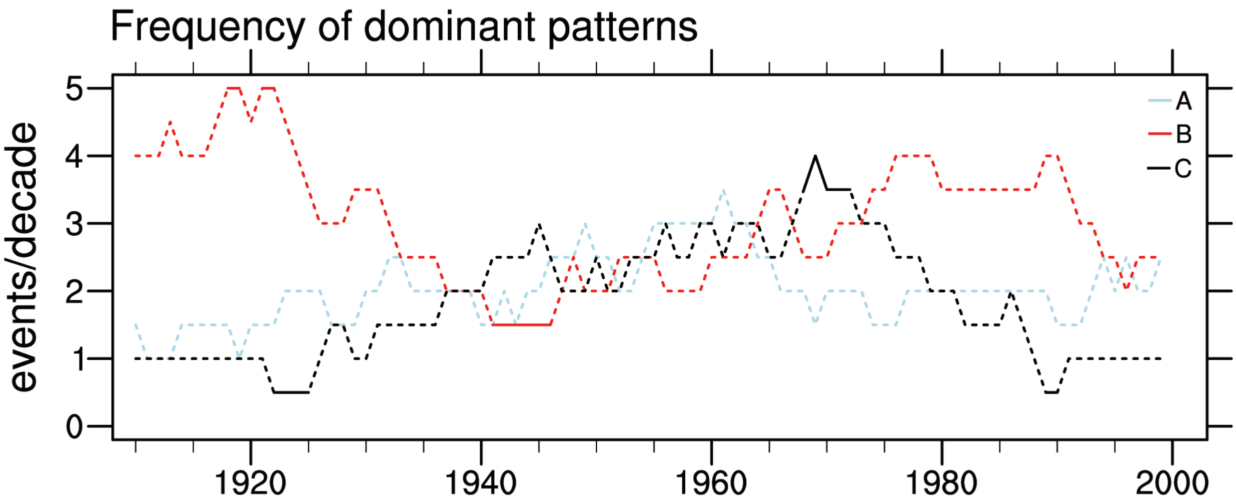

Figure S8. Running average of the number of events in the JFM precipitation clusters A–C per decade for the period 1901–2010. (NB: the value for each decade is plotted with the year at the center of the decade.) Solid lines indicate periods when the number of events is significant at the 5% significance level (as estimated by Monte Carlo testing).

Table S1. Years in clusters A–E, clustered according to JFM precipitation during the period 1901–2010.

Pattern A	1901, 1909, 1917, 1924, 1930, 1933, 1940, 1942, 1952, 1954, 1956, 1959, 1964, 1965, 1971, 1980, 1985, 1987, 1991, 2003, 2004, 2006, 2009
Pattern B	1902, 1904, 1906, 1910, 1913, 1914, 1915, 1916, 1922, 1923, 1926, 1927, 1928, 1931, 1939, 1946, 1948, 1957, 1958, 1962, 1968, 1970, 1974, 1975, 1981, 1982, 1984, 1986, 1988, 1994, 1995, 1999, 2007, 2008
Pattern C	1912, 1919, 1936, 1937, 1941, 1947, 1951, 1955, 1960, 1963, 1966, 1969, 1972, 1977, 1978, 1979, 1996, 2001, 2010
Pattern D	1905, 1907, 1908, 1911, 1918, 1925, 1929, 1932, 1934, 1935, 1943, 1944, 1945, 1950, 1953, 1961, 1967, 1973, 1976, 1983, 1997, 1998, 2005
Pattern E	1903, 1920, 1921, 1938, 1949, 1989, 1990, 1992, 1993, 2000, 2002